

Effect of sintering temperature on the microstructure and optical properties of Mn: CaF₂ transparent ceramics



Ling Liu ^a, Jinghong Song ^b, Weiwei Li ^a, Bingchu Mei ^{a,*}, Liangbi Su ^c, Y. Wang ^d

^a State Key Laboratory of Advanced Technology for Materials Synthesis and Processing, Wuhan University of Technology, 122 Luoshi Road, Wuhan 430070, China

^b Center of Materials Research and Analysis, Wuhan University of Technology, Wuhan 430070, China

^c Key Laboratory of Transparent and Opto-Functional Advanced Inorganic Materials, Shanghai Institute of Ceramics, Chinese Academy of Sciences, Shanghai 201800, China

^d School of Science, China University of Geosciences, Beijing 100083, China

H I G H L I G H T S

- Mn: CaF₂ ceramics were fabricated by hot pressing method.
- The sintering temperature affected densification and microstructure.
- Mn: CaF₂ ceramic sintered at 900 °C showed excellent optical properties.

A R T I C L E I N F O

Article history:

Received 13 May 2017

Received in revised form

18 October 2017

Accepted 23 October 2017

Available online 27 October 2017

Keywords:

Hot pressing

Mn

CaF₂ ceramic

Densification

Microstructure

A B S T R A C T

5 at.% Mn: CaF₂ nanoparticles were used to fabricate transparent Mn: CaF₂ ceramics by hot pressing method at the sintering temperature varying from 700 °C to 1000 °C. The microstructure and optical transmittance of the samples were characterized by FE-SEM and UV–Vis-IR spectrophotometer. It was found that the average grain size of Mn: CaF₂ ceramics increased with the increase of sintering temperature, whereas the relative density firstly increased and then decreased. The highest density of Mn: CaF₂ ceramic reached 99.13% at 900 °C, and its average grain size was about 1.95 μm. The best in-line transmittance was at 900 °C, with transmittance being about 51.49% at 640 nm and 90.2% at 2000 nm, respectively. The excitation and emission spectra of Mn: CaF₂ ceramic were also measured and discussed.

© 2017 Elsevier B.V. All rights reserved.

1. Introduction

Thermoluminescence (TL) materials have been widely used to measure absorbed radiation doses in the areas of clinical, personal and environmental monitoring [1–3]. In the TL processes [1], solid-state inorganic materials produce electron–hole pairs after being irradiated by some kind of radiation such as X-rays, gamma rays, beam of electron and cosmic rays, etc. The electrons and holes are separately trapped at defects, creating a metastable state. When these materials are heated, trapped electrons can be de-captured and entrapped in the hole traps, which causes a light emission by

means of electron–hole recombination.

Calcium fluoride (CaF₂) has gained much attention in the field of thermoluminescence materials, because it has a wide-spread energy band gap values in the range 10–11 eV [4,5]. As a result, probability of the electron re-trapped or de-trapped range is high, whenever ionizing radiation interacts with them. Furthermore, it exhibits a face-centred cubic lattice which can accept many impurities such as transition metal or rare-earth metal ions so that basic dosimetric properties (i.e. sensitivity, dose response, fading, etc.) can be improved. CaF₂ doped with different impurities such as Dy [6], Tm [7], Eu [8] and Mn [9] have been extensively studied earlier. Among these materials, Mn: CaF₂ is the most suitable material for environmental dosimetry and is commercially available as a TLD-400 from Harshaw Chemical Company [10,11]. It shows a high sensitivity and linear response to the radiation dose in an

* Corresponding author.

E-mail address: bcmeilab@163.com (B. Mei).

extremely wide range of doses, from 0.5 mGy to about 10^3 Gy [12]. Besides, it has a single thermoluminescence peak about 260 °C which is very stable at room temperature. Owing to the advantages described above, Mn: CaF₂ seems to be of great importance to investigate.

Recently, most reports about Mn: CaF₂ are either on polycrystalline powder [13] or single crystal [14], but there are only a few reports on Mn: CaF₂ transparent ceramics. Transparent ceramics are of great interest, because its extended advantages over single crystals: larger doping concentration with controllable distribution in the material volume, scalability to large size, low fabrication cost, good mechanical and thermal properties [15,16]. In addition, S.G. Singh et al. [17,18] had found that Mn: CaF₂ transparent ceramics had superior luminescence properties at relatively higher temperatures than the single crystal, and a better sensitivity to lower doses of gamma than the polycrystalline powder samples. Unfortunately, the obtained Mn: CaF₂ transparent ceramic showed a relatively low transmittance which was about 50% above 800 nm and 64% at 2000 nm. It is necessary to fabricate Mn: CaF₂ transparent ceramics with better optical properties for practical application.

In the present study, Mn: CaF₂ ceramics were fabricated by hot pressing method at different sintering temperatures. The microstructure, relative density, optical transmittance and photoluminescence spectrum were investigated. Therefore, our findings provide an optimal sintering condition to improve the transmittance of Mn: CaF₂ ceramics.

2. Experimental

2.1. Nanoparticle synthesis

Mn: CaF₂ nanoparticles were synthesized by co-precipitation method. The starting materials hydrate calcium nitrate (99.9%), manganese (II) chloride tetrahydrate (99.9%), and hydrate potassium fluoride (99.9%) of analytical (AR) grade were used as received without further purification. The weights of these reagents were determined according to the chemical formula Ca_{0.95}Mn_{0.05}F₂. Firstly, a certain amount of Ca(NO₃)₂·4H₂O and MnCl₂·4H₂O were dissolved in the deionized water to make a 1 mol/L cationic solution. The same molar concentration of KF aqueous solution was added dropwise to the cationic solution at the rate of 6 ml/min while stirring continuously for 30 min. The mixture aqueous solution was stayed for 3 h at room temperature for completion of the reaction. Then the obtained precipitates were centrifuged at 11000 rpm for 10 min and washed several times with deionized water. Finally, the products were dried at 80 °C for 24 h in an oven and lightly crushed in an agate mortar.

2.2. Ceramics fabrication

The Mn: CaF₂ transparent ceramics were fabricated by hot pressing method. The nanoparticles were filled into a high density graphite mold (inner diameter: 16 mm) without any treatment, and sintered at 700 °C, 800 °C, 900 °C and 1000 °C respectively in a vacuum environment under uniaxial pressure of 30 MPa. The heating rate was 10 °C/min and the soaking time was 1 h. Finally, the ceramic samples were mechanically mirror polished on both surfaces for microstructural and optical characterizations.

2.3. Measurements

The nanoparticles and ceramic sintered at 900 °C for 1 h were characterized for the phase identification by X-ray diffraction (XRD, D/Max-RB, Rigaku, Tokyo, Japan) measurement using Cu K α

radiation source ($\lambda = 1.54056$ Å). The 2θ for all data ranged from 20° to 80° with a step size of 0.02°. The surface morphology of nanoparticles was observed by Field-emission Scanning electron microscope (FE-SEM, HitachiS4800, Tokyo, Japan) which was also used to measure the microstructure of the fracture surface of ceramics sintered at different temperatures. The average grain size was measured from the SEM pictures using the Nano measurer software. The relative densities of ceramics were measured by Archimedes method with the theoretical density of the doped sample as 3.201 g/cm³. The optical transmittance of Mn: CaF₂ transparent ceramics with a thickness of 2 mm, was measured by a spectrophotometer (Lambda 750, PerkinElmer, USA). The excitation and emission spectra of Mn: CaF₂ sintered at 900 °C were recorded using a spectrofluorometer (FLS920, Edinburgh, UK) with a 900 W Xenon lamp as the excitation source. All measurements were performed at room temperature.

3. Results and discussion

The XRD patterns of Mn: CaF₂ nanoparticles and ceramic sintered at 900 °C for 1 h are presented in Fig. 1. Compared with standard XRD patterns (PDF#35–0816), all the peaks can be well indexed to a cubic phase (fluorite-type structure) of CaF₂ and there are no any second phase appeared. The result indicates that the structure of CaF₂ was not altered by doping with Mn²⁺ ions. It can be clearly seen that the full width at half maximum (FWHM) of the ceramic sintered at 900 °C was much narrower than the powder, and its diffraction peak intensity was stronger which demonstrated an increase of crystallinity after sintering. The crystallite size of the nanoparticle was calculated using the Scherrer equation:

$$L = 0.89\lambda / [\Delta(2\theta) \times \cos(\theta)] \quad (1)$$

Where λ is the diffractometer wavelength, 2θ is the position of the peak and $\Delta(2\theta)$ is the peak width at half maximum, corrected from the instrumental broadening. The average size of Mn: CaF₂ nanoparticles was about 28 nm.

Fig. 2 shows the SEM micrograph of the Mn: CaF₂ nanoparticles. The Mn: CaF₂ nanoparticles exhibited nearly spherical morphology, which possessed good homogeneity in a large scale accompanied with a certain extent of agglomeration. The average particle size observed by SEM was about 40 nm, which was larger than the

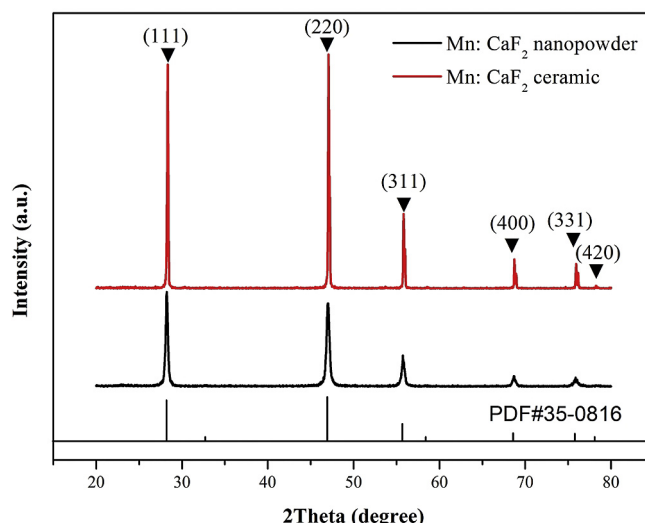


Fig. 1. XRD patterns of Mn: CaF₂: (a) nanoparticle; (b) 900 °C HP-sintered ceramic.

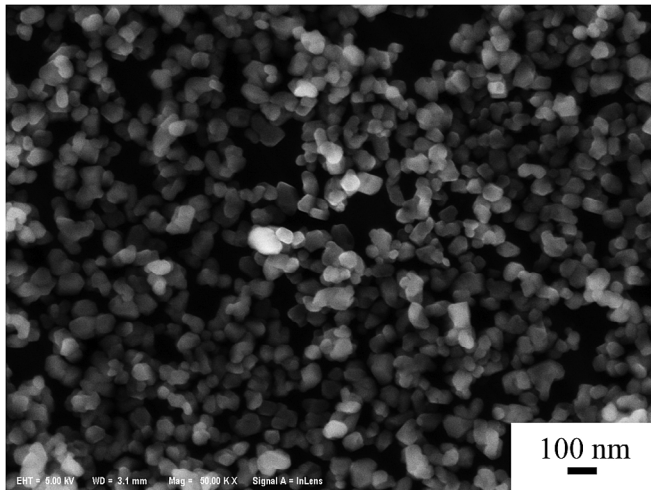


Fig. 2. SEM image of the Mn: CaF₂ nanoparticles.

average size calculated from XRD patterns. This result may be caused by nonideality of real crystals (defects, difference of the chemical composition of the surface layer, etc.) and aggregation processes [19]. These nanocrystalline powders showed good dispersibility and were useful for the preparation of high quality Mn: CaF₂ transparent ceramics.

The microstructures of Mn: CaF₂ ceramics sintered at different temperatures are shown in Fig. 3. When the sintering temperature risen from 700 to 1000 °C, the distinctive changes were the grain

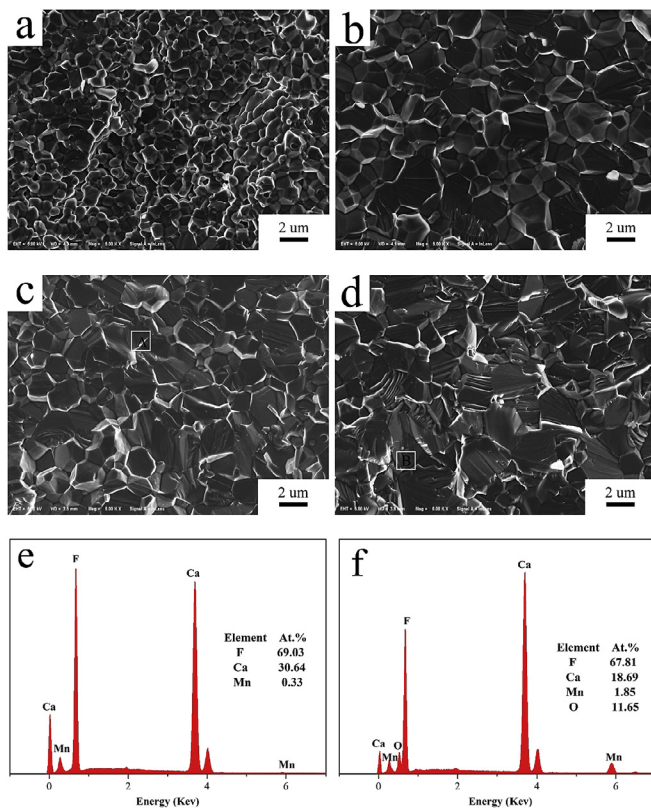


Fig. 3. SEM images of the fracture surface of Mn: CaF₂ ceramics sintered at (a) 700 °C, (b) 800 °C, (c) 900 °C, (d) 1000 °C; (e) EDS spectrum from the square box 'A' in (c), (f) EDS spectrum from the square box 'B' in (d).

size and the number of pores. In general, densification works through particle rearrangement and plastic flow at the particle contacts at the initial stage of sintering [20]. As shown in Fig. 3(a), some particles yielded plastically at their contact points and its contact area increased by neck growth. Therefore, large agglomerate pores, some small grains without clear grain boundaries and a loose structure can be observed. It indicated that the sample was insufficiently sintered and had a lower density which was supported by the relative density value of 85.45% displayed in Fig. 4. At the intermediate stage of sintering (Fig. 3(b)), large pores were eliminated from the pore channels to grain boundary and the grain size increased mainly through grain sliding. A relatively well developed microstructure and fewer residual pores can be observed in Fig. 3(b). At the last stage of sintering, matter can be transported along the grain boundaries onto the surface of the spherical voids, thereby enhancing grain growth [21]. When the sample was sintered at 900 °C, no obvious pores can be observed at the grain boundaries or inside the grains (see Fig. 3(c)). Besides, the structure became more compact and much denser composed of grains with uniform size. Both intergranular and transgranular fracture features can be observed in Fig. 3(b) and (c), and intergranular fracture was the leading fracture mode. Increasing the sintering temperature up to 1000 °C, grain growth rate accelerated, leading not only to a larger average grain size but also to the formation of intragranular pores. And intragranular pores are hard to be removed and have a bad effect on the optical transmittance of ceramics, because residual pores are widely known as strong light-scattering centers.

The EDS spectra were used to analyze the elements in the selected areas, and the results are shown in Fig. 3(e) and (f). For the main phase the elements Ca, Mn, and F were found by EDS detection, whereas the extra element O is observed in Fig. 3(f), and the manganese content remarkably increases. It is supposed that manganese oxides formed at grain boundaries and fell out of the solid solution as the secondary phase at higher temperature [22]. The impurities were generated due to the diffusion of oxygen at higher temperature [23]. The oxygen was mainly from the decomposition of residual nitrate radical in nanopowders. So the precipitates should be washed several times to eliminate nitrate radical as possible. Sils et al. [22] reported that the formation of oxide phase(s) would depend on the temperature and time. As a result, the fabrication of Mn: CaF₂ transparent ceramics should be at an appropriate sintering temperature to prevent the oxidation of manganese. Moreover, the heating rate should be controlled to

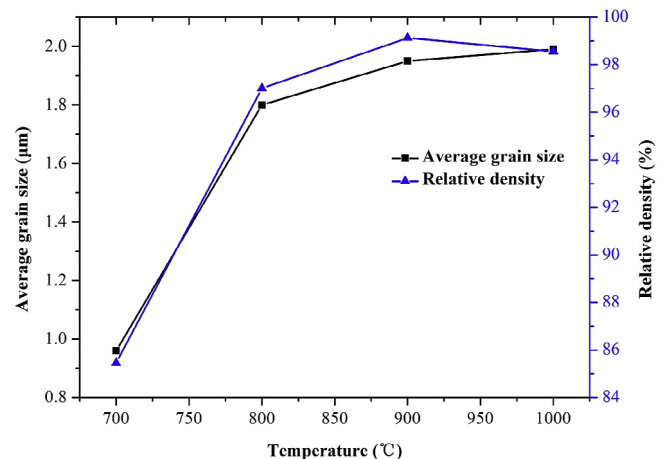


Fig. 4. Relative density and average grain size of Mn: CaF₂ ceramics sintered at different temperatures.

ensure the sufficient pore elimination.

The influences of sintering temperature on the densification and grain growth were analyzed by the density and grain size measurements (Fig. 4). The average grain size was measured by the linear intercept method [24], it was found to be 0.96 μm , 1.80 μm , 1.95 μm and 1.98 μm for the sintering temperatures of 700 $^{\circ}\text{C}$, 800 $^{\circ}\text{C}$, 900 $^{\circ}\text{C}$ and 1000 $^{\circ}\text{C}$, respectively. As the temperature increased from 700 $^{\circ}\text{C}$ to 800 $^{\circ}\text{C}$, the relative density of the specimen increased rapidly, from 85.45% to 97.01%. The sharp densification rate occurred because plastic deformation was the dominant mechanism in this process. It is an instantaneous densification mechanism and is related to significant volume shrinkage [25]. The relative density increased slowly with the increasing of temperature above 800 $^{\circ}\text{C}$, and reached a maximum of 99.13% at 900 $^{\circ}\text{C}$. The densification rate decreased, attributed to its fewer number of fast diffusion paths (i.e., grain boundaries) intersecting each pore [26]. Then the relative density decreases to 98.56% at 1000 $^{\circ}\text{C}$. Hence, increasing the sintering temperature to a certain extent favors densification.

Fig. 5 shows a photograph of mirror-polished Mn: CaF₂ ceramics sintered at different temperatures. It should be noteworthy that the ceramic sintered at 900 $^{\circ}\text{C}$ had high transparency and the letters under the ceramic can be seen distinctly. Generally, porosity and the scattering of light at grain boundaries were identified as the most important factors governing the final transmittance of transparent ceramics. The transmittance can be accurately calculated according to equation [27]:

$$T = (1 - R_s) \exp(-\gamma d) \quad (2)$$

$$R_s = 2R' / (1 + R') \quad (3)$$

$$R' = [(n-1)/(n+1)]^2 \quad (4)$$

Where R_s describes the reflection losses at the two sample surfaces, γ is the total scattering coefficient, d is the transparent ceramic thickness, and n is the refractive index of fluorite optical materials. The refractive index n in materials with cubic symmetry is the same in all directions.

Fig. 6 shows the in-line transmittance of Mn: CaF₂ ceramics sintered at different temperatures. A zero transmittance of all samples can be observed at wavelengths ranging from 200 to 420 nm. The strong absorption may be the result of crystal defect and Mn²⁺ absorption in a CaF₂ lattice [28–30]. The sample sintered

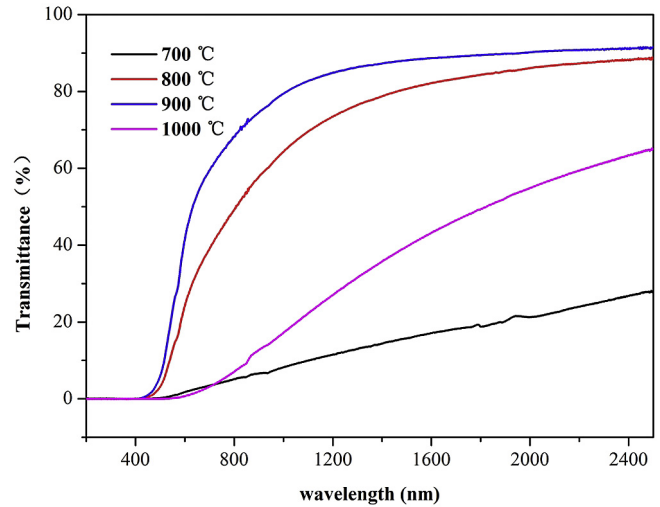


Fig. 6. In-line transmittance spectra of Mn: CaF₂ ceramics sintered at different temperatures for 1 h (2.0 mm thickness).

at 700 $^{\circ}\text{C}$ showed the lowest transmittance compared with the samples sintered at other temperatures. When the sintering temperature increased to 800 $^{\circ}\text{C}$, the transmittance of sample increased sharply, reached about 31.54% at the wavelength of 640 nm and 86.06% at the wavelength of 2000 nm, respectively. The highest in-line transmittance was obtained when the sample was sintered at 900 $^{\circ}\text{C}$. It reached about 51.49% at 640 nm and 90.2% at 2000 nm, while the theoretical transmittance was calculated to be about 93.86% at 640 nm and 94.08% at 2000 nm. The different optical losses can be explained by Rayleigh formula [31]. For smaller wavelength (λ), the scattering intensity is greater, which results in the decrease of transmittance. The transmittance of the specimen sintered at 1000 $^{\circ}\text{C}$ decreased a lot, ascribed to intragranular pores and secondary phase (see Fig. 3(f)). Therefore, a sintering temperature of 900 $^{\circ}\text{C}$ was adequate to obtain Mn: CaF₂ transparent ceramics with high transparency and a desired microstructure.

Fig. 7 displays the excitation and emission spectra of Mn: CaF₂ ceramic sintered at 900 $^{\circ}\text{C}$ for 1 h. A series of characteristic excitation signals appeared in the excitation spectrum for the 508 nm emission. The several bands were centered at 318, 336, 395, 408, and 442 nm which were corresponding to the transition from

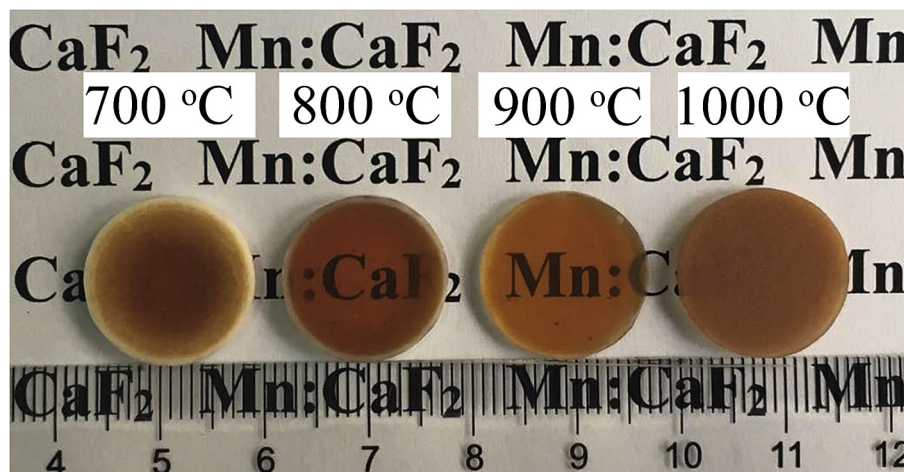


Fig. 5. Photograph of Mn: CaF₂ ceramics sintered at different temperatures for 1 h under vacuum environment.

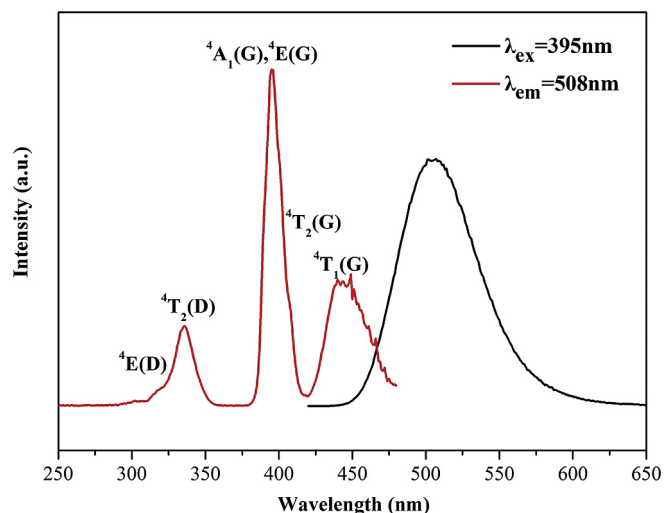


Fig. 7. Excitation and emission spectra of Mn: CaF₂ ceramic sintered at 900 °C.

${}^6A_1(S)$ ground state to the ${}^4E(D)$, ${}^4T_2(D)$, [${}^4A_1(G)$, ${}^4E(G)$], ${}^4T_2(G)$, and ${}^4T_1(G)$ excited states, respectively [32]. Under 395 nm excitation, the emission of Mn: CaF₂ sample was in the green spectral range peaking at 508 nm. The broad emission band can be attributed unambiguously to the spin forbidden transition of ${}^4T_{1g}({}^4G) \rightarrow {}^6A_{1g}({}^6S)$ of Mn²⁺, suggesting the only octahedral coordination of Mn²⁺ ions with surrounding F⁻ ions, which was consistent with previous reports [30,32].

4. Conclusions

Transparent Mn: CaF₂ ceramic was fabricated by hot pressing method. The effect of sintering temperature on the microstructure and optical transmittance of Mn: CaF₂ ceramic was investigated. The sample sintered at 900 °C showed clean grain boundaries structure and no impurities were detected, whereas the secondary phase appeared in the sample sintered at 1000 °C. The result confirms it is essential to control the heating rate at an appropriate sintering temperature to ensure the sufficient pore elimination and suppress oxide. The best Mn: CaF₂ transparent ceramic was made by sintering at 900 °C for 1 h, which was dense and homogeneous in structure with the average grain size of about 1.95 μm and the maximum density of 99.13%. The in-line transmittance of the sample with the thickness of 2 mm was 51.49% at 640 nm and 90.2% at 2000 nm, respectively. The main emission peak of Mn: CaF₂ ceramic was centered at about 508 nm, which can be attributed to the spin forbidden transition of ${}^4T_{1g}({}^4G) \rightarrow {}^6A_{1g}({}^6S)$ of Mn²⁺.

Acknowledgement

This work was financially supported by the National Natural Science Foundation of China (No.51432007).

References

- [1] T. Kron, *Radiat. Prot. Dosim.* 85 (1999) 333–340.
- [2] S.W.S. McKeever, *Thermoluminescence of Solids*, Cambridge University Press, 1985.
- [3] P.P. Pal, J. Manam, *Mat. Sci. Eng. B* 178 (2013) 400–408.
- [4] M.S. Bhadane, K. Hareesh, S.S. Dahiwal, K.R. Sature, B.J. Patil, et al., *Nucl. Instrum. Meth. Phys. Res. B* 386 (2016) 61–69.
- [5] A.K. Bakshi, B. Dhabeekar, N.S. Rawat, S.G. Singh, V.J. Joshiet, et al., *Nucl. Instrum. Meth. Phys. Res. B* 267 (2009) 548–553.
- [6] M. Zahedifar, E. Sadeghi, S. Harooni, *Nucl. Instrum. Meth. Phys. Res. B* 291 (2012) 65–72.
- [7] D.A.A.D. Vasconcelos, V.S.M. Barros, H.J. Khoury, V.K. Asfora, R.A.P. Oliveira, *Radiat. Phys. Chem.* 121 (2016) 75–80.
- [8] F. Nakamura, T. Kato, G. Okada, N. Kawaguchi, K. Fukuda, T. Yanagida, *Ceram. Int.* 43 (2017) 604–609.
- [9] B. Zorko, S. Miljanić, B. Vekić, M. Stuhc, S. Gobec, et al., *Radiat. Prot. Dosim.* 119 (2006) 300–305.
- [10] M. Danilkin, A. Lust, M. Kerikmäe, V. Seeman, H. Mändar, et al., *Radiat. Meas.* 41 (2006) 677–681.
- [11] M. Topaksu, V. Correcher, J. Garcia-Guinea, *Radiat. Phys. Chem.* 119 (2016) 151–156.
- [12] D.L. Fehl, D.J. Muron, B.R. Suijka, D.W. Vehar, L.J.L. Jr., et al., *Rev. Sci. Instrum.* 65 (1994) 3243–3251.
- [13] M. Zahedifar, E. Sadeghi, Z. Mohebbi, *Nucl. Instrum. Meth. Phys. Res. B* 274 (2012) 162–166.
- [14] R. Nakata, K. Kohno, M. Sumita, E. Higuchi, *J. Phys. Soc. Jpn.* 41 (1976) 470–474.
- [15] X. Liu, B. Mie, W. Li, Z. Sun, Z. Liu, et al., *Ceram. Int.* 42 (2016) 13285–13290.
- [16] M.S. Akchurin, T.T. Basiev, A.A. Demidenko, M.E. Doroshenko, P.P. Fedorov, et al., *Opt. Mater* 35 (2013) 444–450.
- [17] S.G. Singh, S. Sen, G.D. Patra, S. Bhattacharya, A.K. Singh, et al., *Nucl. Instrum. Meth. Phys. Res. B* 287 (2012) 51–55.
- [18] S.G. Singh, S. Sen, G.D. Patra, S.C. Gadkari, *J. Lumin.* 166 (2015) 222–226.
- [19] A. Safronikhin, H. Ehrlich, G. Lisichkin, *J. Alloys Compd.* 694 (2017) 1182–1188.
- [20] S.F. Wang, J. Zhang, D.W. Luo, F. Gu, D.Y. Tang, et al., *Prog Solid State Chem.* 41 (2013) 20–54.
- [21] Y. Zhang, A. Song, D. Ma, X. Zhang, M. Ma, et al., *J. Alloys Compd.* 608 (2014) 304–310.
- [22] P.D. Sahare, M. Singh, P. Kumar, *Radiat. Meas.* 80 (2015) 29–37.
- [23] J. Sils, E. Radzhabov, M. Reichling, *J. Phys. Chem. Solids* 68 (2007) 420–425.
- [24] H. Abrams, *Metallography* 4 (1971) 59–78.
- [25] M. Chen, J. He, Y. Zhang, Z. Ding, J. Luo, *Ceram. Int.* 43 (2017) 1775–1780.
- [26] E.H. Slamovich, F.E. Lange, *J. Am. Ceram. Soc.* 76 (1993) 1584–1590.
- [27] R. Apetz, M.P.B. Bruggen, *J. Am. Ceram. Soc.* 86 (2003) 480–486.
- [28] J. Wang, C.C. Wang, Q.J. Li, Y. Yu, J. Zhang, et al., *Mat. Sci. Eng. B* 188 (2014) 31–34.
- [29] K. Chakrabarti, J. Sharma, V.K. Mathur, J.H. Barkyoub, *Phys. Rev. B* 51 (1995) 16541–16548.
- [30] S.W.S. McKeever, B. Jassemnejad, J.F. Landreth, M.D. Brown, *J. Appl. Phys.* 60 (1986) 1124–1130.
- [31] A. Ikesue, K. Yoshida, T. Yamamoto, I. Yamaga, *J. Am. Ceram. Soc.* 80 (1997) 1517–1522.
- [32] P.J. Alonso, R. Alcalá, *J. Lumin.* 21 (1980) 147–152.